Accepted by International Journal of Fatigue

Relationship between fatigue parameters and fatigue crack growth in PMMA bone cement

E. M. Sheafi[1], K.E. Tanner[1,2]

[1] *Biomedical Engineering Division, School of Engineering, University of Glasgow, Glasgow, G12 8QQ, UK*
[2] *Now at School of Engineering and Materials Science, Queen Mary University of London, Mile End Road, London, E1 4NS*

ARTICLE INFO

Article History:
Received 20 April 2018
Received in revised form 2 November 2018
Accepted 9 November 2018

Keywords:
Polymethylmethacrylate
Bone cement
Fatigue
Fatigue crack growth
CT specimen

ABSTRACT

Poly(methyl methacrylate) (PMMA) bone cement is used to anchor the majority of total joint replacements (TJRs). Many brands of cement are used, both with and without the addition of antibiotics to reduce the risk of infection. The present study involved determination of various parameters in tensile fatigue loading:

1) energy absorbed (U) vs number of loading cycles (N) and creep strain (e) vs N, during fatigue tests on specimens of an antibiotic-containing cement (SmartSet GHV) and a plain cement (CMW1) and
2) crack length (a) vs fatigue loading cycles (N) and crack growth rate (da/dN) vs Mode I stress intensity factor range (DK_I), during Fatigue Crack Propagation (FCP) tests.

In the fatigue tests, four different sample types (round, machined; round, directly moulded; rectangular, machined, and rectangular, directly moulded) and tension-tension loading were used. In the FCP tests, compact tension specimens under tension-tension loading were used.

It was found that there were limited effects of sample type, except at the highest stress levels, but that these two cements had different rates of crack propagation. These differences were reflected in the fracture surfaces with SmartSet GHV showing accumulation of opacifier around the particles and crack progression around the intial beads, while for CMW1 the opacifier was evenly distributed and the cracks went through the initial beads.

1. INTRODUCTION

In the majority of total joint replacement (TJRs), poly(methyl methacrylate) (PMMA) bone cement is used as the grouting agent to anchor one or both of the components [19]. Fatigue fracture at the cement/bone interface, within the cement layer itself, and/or at the cement-prosthesis interface has been cited as a cause of or implicated in loosening of the prosthesis *in vivo* [13,39]. Therefore, there are many reports in the literature on *in vitro* determination of fatigue properties of bone cement, with the results typically presented as number of cycles to fracture (N_f) at specified applied fatigue stress level(s) usually in the form of S-N or Wöhler curves. These results are influenced by many factors [22], such as composition of the cement [12,23,30], specimen configuration [20,21,35,36], type of applied stress [35,36], and specimen surface finish [37]. Additionally, there have been a number of literature reports on the *in vitro* determination of fatigue crack propagation (FCP) behaviour of bone cement [4,8,14,24,28,29,40]. The results are usually presented as crack length (a) vs number of loading cycles (N), at a given applied stress level and/or crack growth rate (da/dN) vs stress intensity factor range, typically Mode I (ΔK_I), at specified fatigue stresses [4,8,10,12]. In many reports morphologies of fracture surfaces at the end of a fatigue test or a FCP test are also presented and used to clarify the mechanisms of failure (for example [8,30]).

In the fatigue testing of bone cement, information on relevant characteristics, such as the energy absorbed by a specimen (U) and the creep deformation (ε) have been reported in only a few studies [14,36]. Wheeler et al. [45] showed that creep movement of cement is beneficial in allowing re-distribution of stresses as would occur with changes in the bone surrounding an implant. Jeffers et al. [14] used acoustic emission to detect crack growth events to elucidate the progresses of cement reaction to loading. Although the fatigue and FCP behaviour of a material are related, in the case of bone cement knowledge of the relationship between these factors is limited. These new results could provide valuable insight into the mechanisms involved in fatigue and FCP of bone cement, informing both crack initiation processes and crack propagation. This knowledge may be used in developing a new generation of bone cements with increased resistance to fatigue loading thus contributing to increased *in vivo* life of cemented TJRs. In the longer term this will reduce the rate of revision surgery and lead to improved patient satisfaction and implant longevity.

The present study has two purposes. The first was to determine the influence of the specimen fabrication method, specimen cross-sectional shape and cement type on energy absorbed per load cycle (U) vs number of load cycles (N) relationship, and the creep strain (ε) vs number of load cycles, as obtained from tension-tension fatigue tests. The second was to determine the influence of cement brand on crack length (a) vs number of load cycles (and, hence, change in crack growth rate (da/dN) versus stress intensity factor), as obtained using compact tension specimens in tension-tension loading. One of these brands (SmartSet GHV) is antibiotic-loaded, used for the vast majority of revision surgery and many primary operations and the other [19].

2. Materials and methods

2.1. Materials

Two different brands of PMMA bone cement were used to evaluate the fatigue behaviour, both produced and supplied by DePuy CMW, Blackpool, UK. For both cements, each pack contains 40g polymer powder and 18.88g liquid monomer that are mixed together and moulded, as described below. Details of the two cements are provided in a previous study [35] but, briefly, the major differences are that in SmartSet GHV, the powder phase constituents include poly(methyl

Corresponding Author: Professor K. E. Tanner, School of Engineering and Materials Science, Queen Mary University of London, Mile End Road, London, E1 4NS, UK e-mail: k.e.tanner@qmul.ac.uk

methacrylate, methacrylate copolymer, P(MMA-MA)) beads, ZrO_2 particles as the radiopacifier and an antibiotic (gentamicin sulphate), whereas in CMW1, the corresponding constituents are poly(methyl methacrylate, PMMA) beads thus no copolymer, $BaSO_4$ particles and no antibiotic. The liquid monomer phase is the same.

2.2. Mixing of cement components

The cement components were mixed at room temperature (21±2°C) using a CEMVAC mixing system (DePuy CMW, Blackpool, UK). The mixing process was performed as per the manufacturer's instructions concentrating on mixing time, waiting time and working time. During mixing, reduced pressure (~ -70 kPa) was applied to the CEMVAC system using mixing speed of about 1 beat/s for a total mixing time of 30-45 seconds. Once the components were mixed, the mixture was left in the mixing system syringe for the waiting time specified by the manufacturer, considering room temperature and cement type.

2.3. Fatigue life measurement specimens

As previously described in Sheafi and Tanner [35,36], the cement mixture was injected into previously prepared PTFE moulds that had either cavities of the required test specimen geometries or oversized cavities. These were either rectangular waisted cavities to produce specimens with rectangular cross sections (R) according to ISO 527-2 (half size) for direct moulding (DM) or rectangular oversized cavities to produce moulded rods that were subsequently machined to size (MM). Similarly, specimens with circular cross sections (C) were prepared according to ASTM F2118-03 [2] using the direct moulding (DM) or moulding and machining (MM) production methods. It should be noted that a later version of this standard (ASTM F2118-14) [3] requires preparing all specimens by direct moulding. In total, for each of the two cement brands, four types of specimens were obtained: RDM, RMM, CDM and CMM. Pressure was applied on the moulds immediately after the injection process, using a hydraulic press, for 20-30 minutes. Prior to testing, the specimens were aged in saline at 37°C for 1 to 6 weeks (7-42 days), ASTM F2118-14 suggests 7 to 60 days, so slightly longer.

Specimens were tested in stress control and at 3Hz under a flow of saline at 37 °C, to model the physiological environment and control the specimen temperature. Testing used a servo hydraulic testing machine (MTS – 858 Mini Bionix® II) and subjected to either tension-tension loading (max stress = 20 MPa; R = 0.1) as reported in Sheafi and Tanner [36] and used by other authors including Harper et al [12] and Tanner et al. [38] or fully reversed tension-compression [37]. While 2-20 MPa is above physiological stress levels, it typically leads to fatigue in less than 100,000 load cycles, allowing specimens to be tested in a sensible time [12,38]. Being a viscoelastic material, and thus liable to heating, the test frequency has to be limited when testing bone cement. At each stress type and level, a minimum of 10 specimens were fatigued to failure, any that had macro-pores (≥1mm) in the fracture surface were discarded and replaced.

The data was collected using the MTS software (TestStar II) that was programmed to record the force and crosshead displacement during loading and the number of cycles to fracture (N_f). The program recorded the fatigue data logarithmically, that is during cycles 1-100, 200-210, 300-310, … 1000-1010, 2000-2010, etc, plus recording the last 1,000 cycles before failure. For each of the recorded loading cycles, 10 data points of the instantaneous force and displacement were recorded. After testing, the force and displacement data for the specimen with median fatigue life for that group was used to generate stress-strain curves (hysteresis loops) for the pre-selected loading cycles and the instantaneous absorbed energy per load cycle (U) was calculated in Microsoft Excel using the Trapezoid Integration Rule for the determination of the area of an enclosed (polygonal) shape, that is of the difference between the loading and the unloading curves, allowing plots of U vs N to be generated. For these median specimens, the fatigue and strain data was used to compare the creep deformation that occurred during loading to give strain (e) vs N graphs. These were used to assess whether creep affects to the fatigue crack growth.

The morphologies of the fractured surfaces were obtained using a scanning electron microscope (SEM, Hitachi, Tokyo, Japan, S4700 FE-SEM) at an acceleration voltage of 5kV on specimens from both cements to compare the topography of the fracture surfaces.

2.4. Fatigue crack growth measurement (CT) specimens

A flat PTFE mould, 3mm thick, with 38mm by 40mm cavities, was used to produce blank specimens by injecting and pressurising the cement mixture into the mould cavities, as described above. After a minimum of 24 hours, the notch and loading holes shown in Fig. 1 were machined in the moulded specimens to produce CT specimens as described by ASTM-E647-13 [1]. The use of a plain rectangular mould and then machining to produce the notches and loading holes simplifies flow leading to more uniform distribution of the cement in the moulds. Similar to the dumbbell specimens, the CT specimens were soaked in saline at 37°C for 1 to 6 weeks before testing. A crack propagation gauge (Model TK-09-CPA01-005/DP, Vishay Precision Group) was glued to the specimen to cover the area where the fatigue crack was expected to grow and connected to an electrical circuit used as an external input to the MTS data logging system. This crack measurement gauge has 20 grid lines (strands) with a distance of 0.25mm between each two adjacent strands, providing a total grid width of 5mm. As each strand fractured the resistance of the gauge increased, the voltage dropped and the time between these step changes indicated the time required for the crack to grow 0.25mm. To electrically isolate the gauge from the flow of the saline solution on the specimen, the gauge was covered by a thin waterproof layer (transparent nail varnish). ASTM E647-13 [1] requires "a pre-crack that has been growing at or below the test load", so a distance of 1mm was left between the "artificial", that is machined, crack tip and the first strand of the gauge to ensure the gauge was measuring crack propagation in the stable region. The setup of the CT fatigue testing protocol is shown in Fig. 2.

For each cement type, a minimum of five specimens were subjected to uniaxial tension-tension cyclic loading at a frequency of 2 Hz until failure. To allow sufficient time to track the crack growth, loading was performed between $0.1P_{max}$ and $0.5P_{max}$ where P_{max} is the force required to break a CT specimen under quasistatic tensile loading. P_{max} was obtained by testing two randomly selected CT specimens from each of the bone cements subjecting them to tensile loading of speed of 1 mm/min until failure, recording the failure force as P_{max}. As with the fatigue testing if a specimen was found to have macro-porosity or other defects on the fracture surface, a replacement specimen was tested. It should be noted that, due to the presence of the pre-cracked knotch accelerating crack initiation and propagation, the maximum applied stress was above that calculated to occur *in vivo* [5,20]. However, due to the presence of the pre-cracked notch accelerating crack initiation and propagation, the aim was only to monitor fatigue crack propagation and its growth rate. Once the fatigue test had started, the data was collected in the manner specified within the selected test procedure, including recording the force, displacement and N against time in conjunction with the sudden changes in voltage. The instantaneous crack length, a, was identified using Eq. (1).

$$a = a_0 + n(\Delta a) \tag{1}$$

where, n is the number of gauge strands broken at a certain stage and Δa is the crack growth increment that represents increase in crack length after the fracture of each strand ($\Delta a = 0.25$ mm).

Once the crack length was obtained at each stage, the crack growth per loading cycle was determined using Eq. (2).

$$\left(\frac{da}{dN}\right)_i = \frac{a_i - a_{i-1}}{N_i - N_{i-1}} \tag{2}$$

where, $\frac{da}{dN}$ is the crack growth rate and i is the strand number (i = 1, 2, 3,..., 20). The Mode I stress intensity factor range (ΔK_I) was determined at each crack increment point according to Eq. (3) [1].

$$\Delta K_I = \frac{\Delta P}{B\sqrt{W}} \frac{\left(2+\frac{a}{W}\right)}{\left(1-\frac{a}{W}\right)^{3/2}} \left[0.886 + 4.64\left(\frac{a}{W}\right) - 13.32\left(\frac{a}{W}\right)^2 + 14.72\left(\frac{a}{W}\right)^3 - 5.6\left(\frac{a}{W}\right)^4\right] \tag{3}$$

where, ΔP is the difference between the maximum and minimum load levels, W is the specimen width, defined as the distance between the centre line of the loading holes and the edge of the sample, B is the specimen thickness, as shown in Fig. 1.

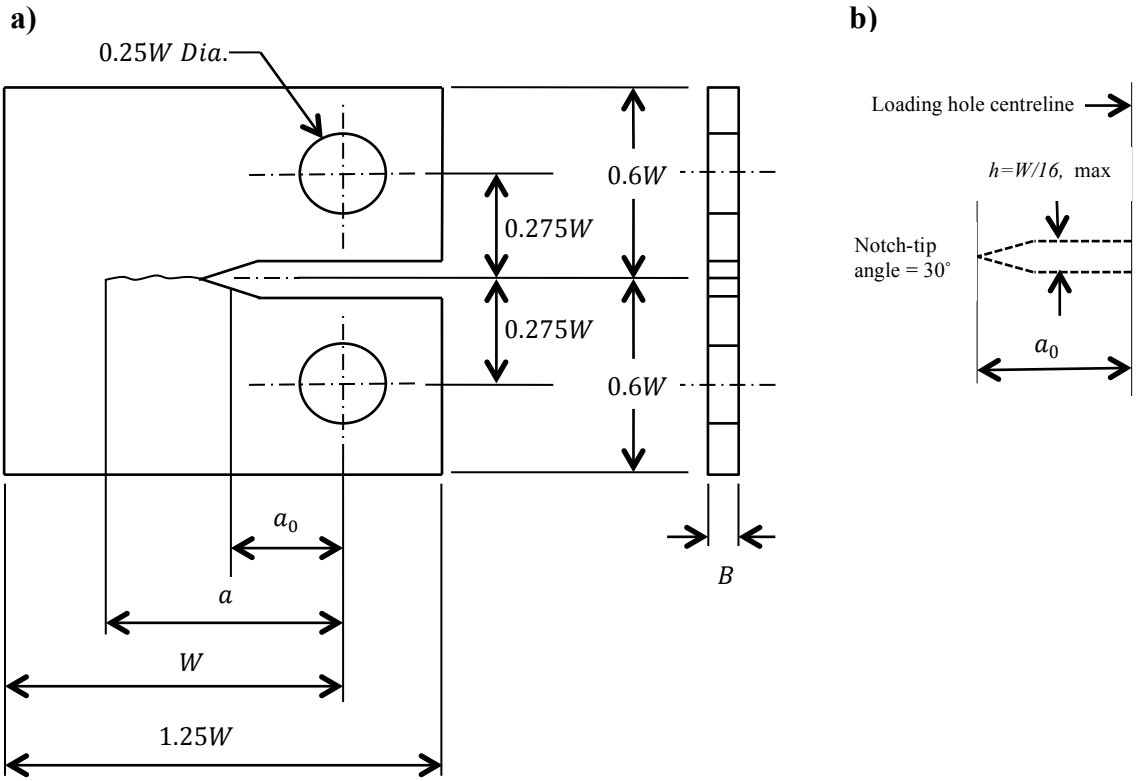

1 Geometry and nominal dimensions of the CT specimen (ASTM-E647-13) [1] used for crack growth rate: **(a)** specimen and **(b)** notch details

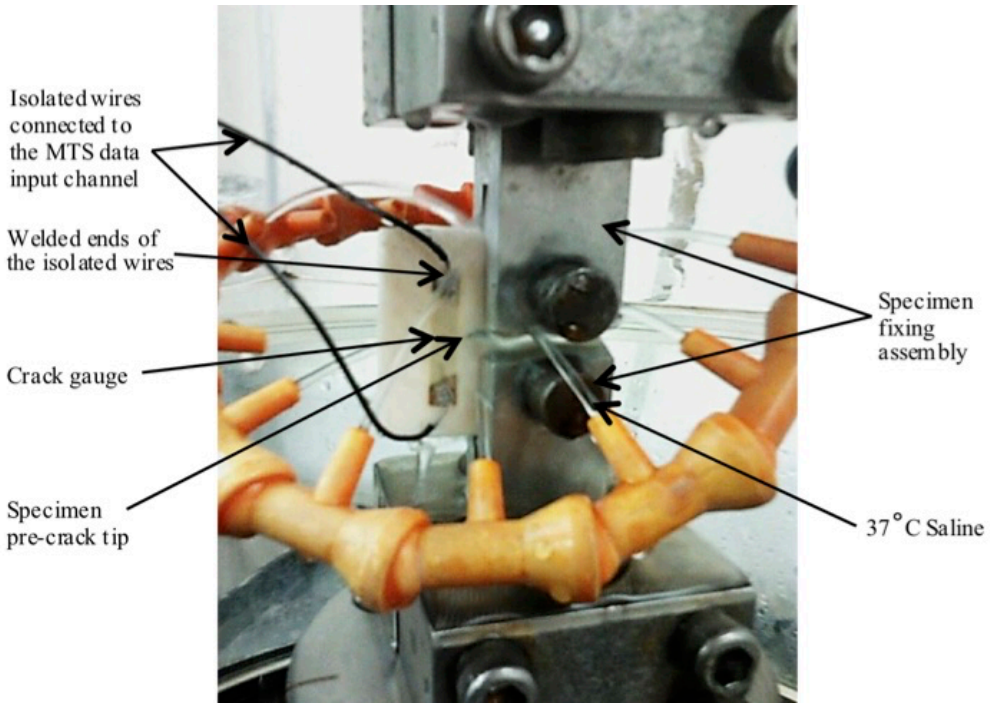

Figure 2 A CT specimen with a crack measurement gauge during testing

Two graphs were generated. The first graph shows the crack length, a, measured by strand breakage, against N, describing the relation between crack growth and loading cycles. The other graph, which has been widely related to the use of the CT specimens, describes the crack propagation rate (da/dN) as a function of the stress intensity factor (ΔK_I). It has been reported that when load amplitude is constant, the stress intensity factor increases with crack propagation for most specimen geometries [6]). It was considered

therefore, the values of the stress intensity range should show an increase as the crack propagates. Paris' power law (Eq. (4)) was subsequently used to compare the findings for the CT specimens. To generate a power law fit, the data was presented on a log-log plot of da/dN versus ΔK_I. The data from the five specimens for each cement was combined and used to generate a single line to allow comparison of the behaviour of the two cements.

$$\frac{da}{dN} = C(\Delta K_I)^m \quad (4)$$

where $\frac{da}{dN}$ is the fatigue crack growth rate, ΔK_I is the stress intensity factor range = $K_{I\,max} - K_{I\,min}$ (maximum and minimum stress intensity factors, respectively) and C and m are material constants.

3. Results

3.1. Estimation of fatigue damage accumulation under fatigue loading

Under tension-tension (Fig. 3) and tension-compression loading (Fig. 4), for each cement, similar absorbed energy behaviour was found for the different specimen types under the various loading regimes. For all the SmartSet GHV specimens, the absorbed energy increased gradually through loading until just before failure when the amount of absorbed energy increased more rapidly, typically by approximately 50% of the initial value (Fig. 3a and 4a). In contrast for the CMW1 specimens, there were minimal changes in energy absorbed per fatigue cycle throughout the testing period until close to failure where the absorbed energy increased only slightly (Fig. 3b and 4b).

Under fully reversed tension-compression, the amount of absorbed energy per loading cycle varied depending on the cement composition, specimen type and stress parameters (Fig. 4). Fatigue longevity was largely controlled by specimen type, however, the gradual increase in the absorbed energy, and thus the increase in fatigue crack length, was more obvious in the SmartSet GHV specimen types than the CMW1 specimens. The SmartSet GHV specimen types showed variations in energy absorbed between each other that was not found for the CMW1 specimens. For SmartSet GHV (Fig. 4a) the variations in the absorbed energy between the four specimen types were seen to be mainly affected by the stress level. At the lower stresses and more physiological stresses of ±12.5 and ±15 MPa, the absorbed energy per loading cycle increased gradually and slowly throughout the testing period. At the higher stress of ±20 MPa, the energy absorption progress in the moulded specimens was similar to that for the lower stress levels whereas in the machined specimens, particularly the circular, the absorbed energy amount started to increase rapidly well before reaching failure. At the highest stress of ±30 MPa, the rapid increase started earlier for all specimen types, but the circular machined specimens provided remarkably higher increases in the energy absorption rate. For CMW1 (Fig. 4b) all specimen types showed similar behaviour, which was steady throughout the fatigue testing period, with minimal changes in energy per loading cycle until very close to failure when the absorbed energy increased obviously. The absorbed energy per loading cycle at the highest stress level of ±30MPa was, however, almost three times higher than the other stress levels, indicating the change from high cycle to low cycle fatigue.

The creep behaviour of the different specimens of these cements tested in tension-tension fatigue is shown in Fig. 5. The creep behaviour of different specimens of the same cement are similar, but again remarkably different for the two cements. Although how much of the apparent "creep" is true creep and how much is damage accumulation by the cement during the fatigue process cannot be stated. Fig. 6 shows SEMs of the fracture surfaces of the two cements showing the accumulation of the zirconia opacifier around the PMMA beads in SmartSet GHV at the fracture surface while opacifier agglomeration does not occur with the barium sulphate in CMW1. It can be seen that for the SmartSet GHV the crack has propagated around the pre-polymerised PMMA beads where the zirconia opacifier has accumulated at these beads and debonding of opacifier has occurred, whereas the fracture has progressed through the pre-polymerised CMW1 beads and the barium sulphate opacifier which is evenly distributed throughout the matrix phase of the cement.

3.2. *Measurement of fatigue crack growth in cements*

As indicated by the changes in absorbed energy, a similar trend of differences in fatigue crack growth behaviour between these two cements was found with the CT specimens in fatigue. The fatigue crack started to propagate in SmartSet GHV specimens earlier (and well before failure), showing slowly increasing crack length with fatigue cycles, in contrast the cracks either did not appear to propagate or propagated at extremely slowly for the CMW1 specimens until close to failure, ending with rapid crack propagation. Over the crack propagation length of 5mm (the width of the crack gauge starting from 1mm after the CT pre-crack tip), all the SmartSet GHV specimens (Fig. 7a) showed similar and constantly accelerating crack growth rate over the last approximately 3mm. CMW1 specimens (Fig. 7b), in comparison, showed no obvious increase in the crack length indicating significantly greater resistance to crack development. However, once the crack initiated in CMW1 specimens rapid crack propagation occurred leading to failure. Table 1 shows the crack lengths at which failure occurred for the CT test specimens. Clearly, SmartSet GHV allowed longer fatigue cracks to grow before reaching the failure point compared to CMW1 so that, in addition to showing fast crack growth, it underwent failure at shorter crack lengths.

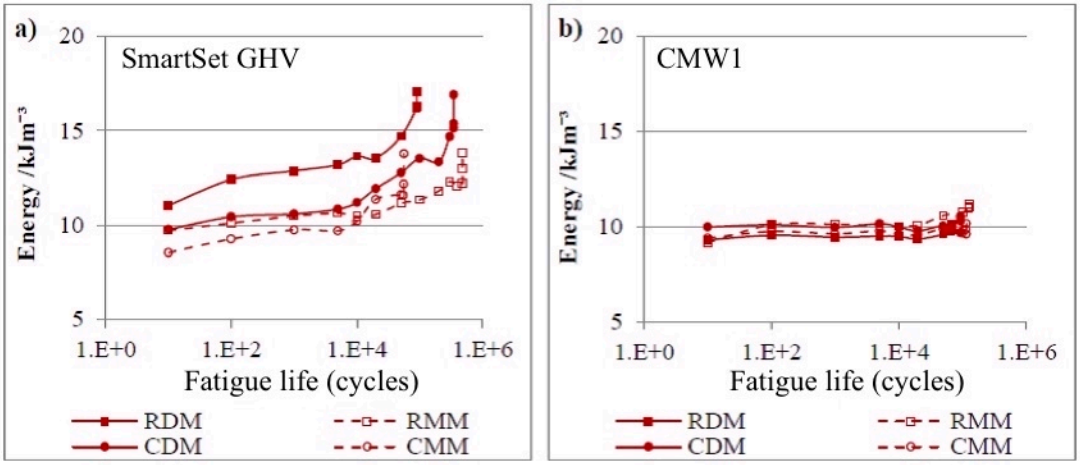

Figure 3 Variations in the absorbed energy per loading cycle for median fatigue life samples for the different specimen types tested in 2-20MPa tension-tension, comparing (a) SmartSet GHV and (b) CMW1 (Reproduced with permission from Sheafi and Tanner, 2015)

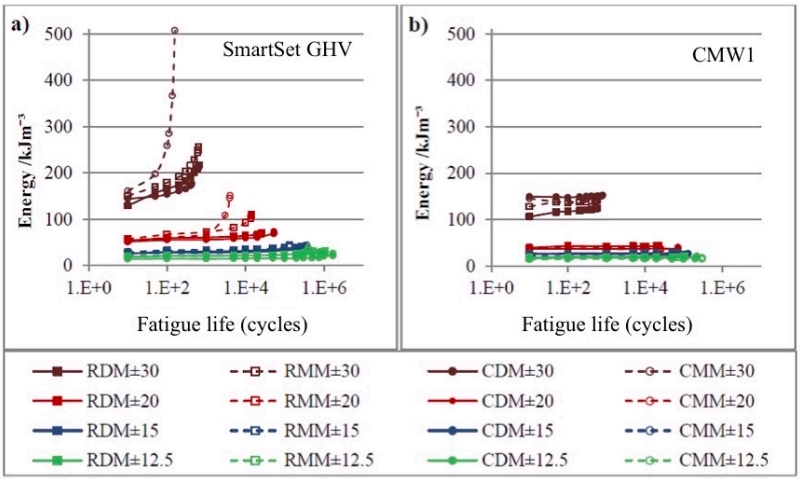

Figure 4 Variations in the increase in absorbed energy per loading cycle for the different specimen types tested in tension-compression, showing (a) SmartSet GHV and (b) CMW1 (note: RDM±30 refers to the RDM specimen type tested at stress levels of ±30 MPa etc.)

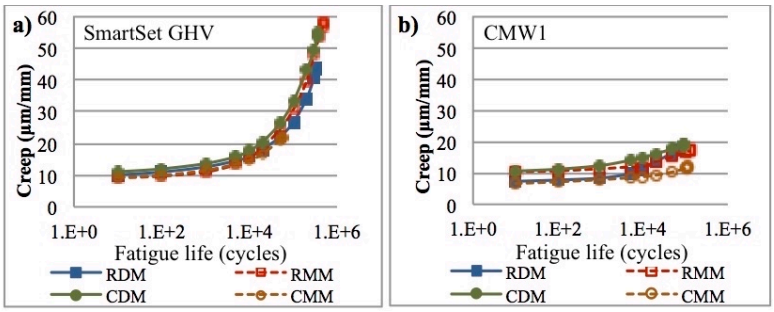

Figure 5 Creep strain behaviour of median fatigue life samples of (a) SmartSet GHV and (b) CMW1 under 2-20 MPa tension-tension fatigue (R=0.1)

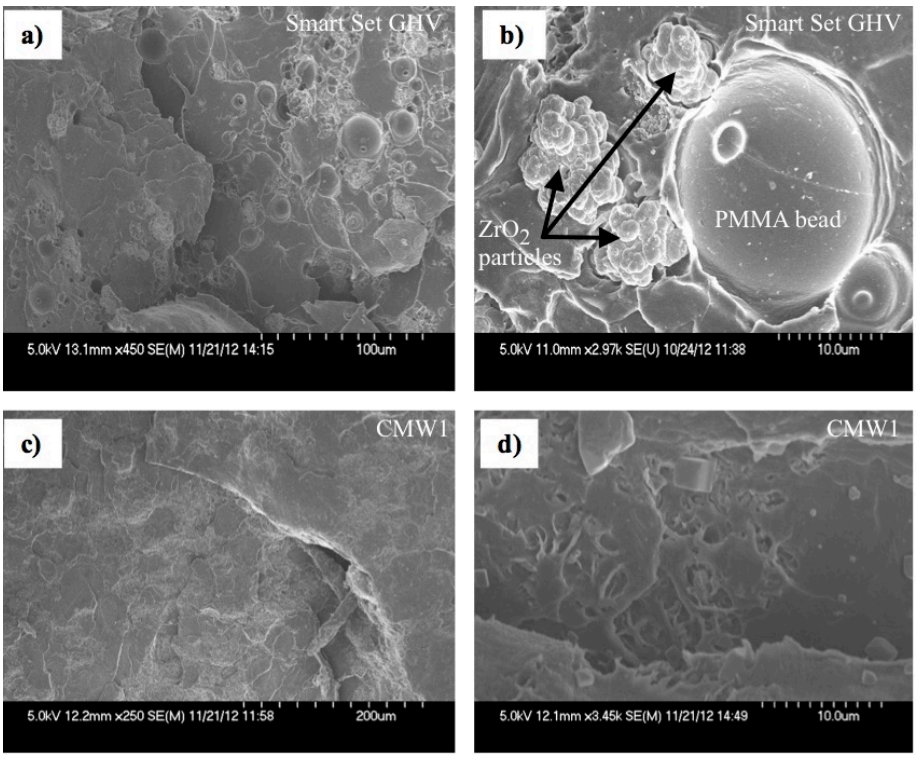

Figure 6 Morphologies of fatigue fracture specimens, under tension-tension loading (a) the disconnection of the P(MMA-MA) beads without being fractured, (b) the interaction between a P(MMA-MA) bead and accumulated ZrO_2 particles for SmartSet GHV (marker bars = 100µm and 10µm, respectively) and (c & d) for CMW1 showing fracture through the individual PMMA beads (marker bars = 200µm and 10µm, respectively)

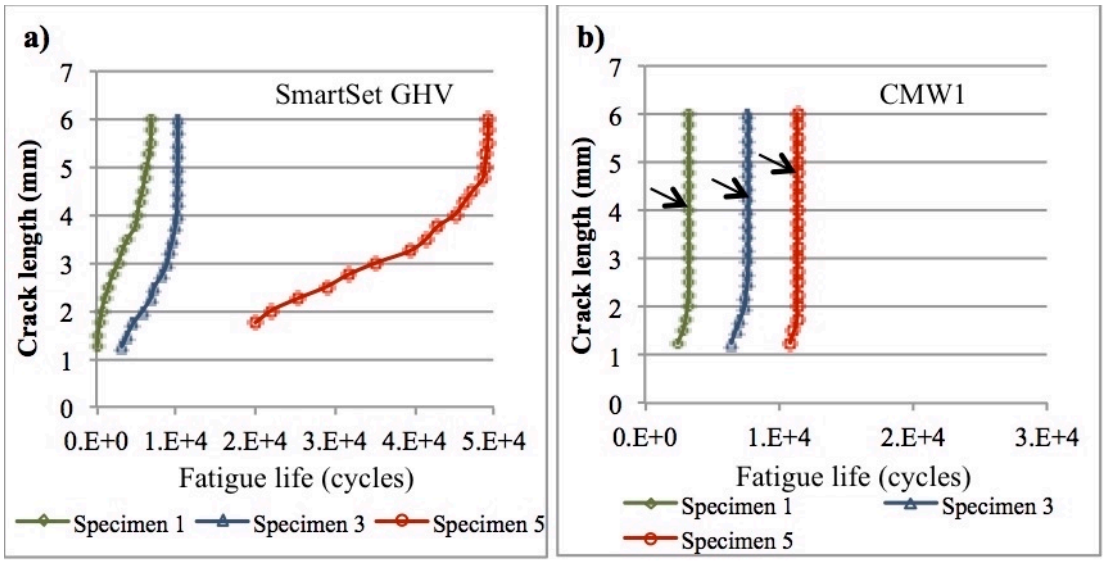

Figure 7 Comparison between the fatigue crack propagation in (a) SmartSet GHV and (b) CMW1 for low (Specimen 1), median (Specimen 3) and high (Specimen 5) performance specimens for each cement – the arrows show early failure points in CMW1

Most of the calculated fatigue crack growth rates were within the required range provided by ASTM E647-13 [1] which recommends $da/dN > 1.0\times10^{-8}$ mm/cycle at constant load amplitude. While the lowest crack growth rates were slightly above this limit for SmartSet GHV specimens (between 2.2×10^{-8} and 2.2×10^{-7} mm/cycle), they were well above the limit for CMW1 specimens (between 1.0×10^{-7} and 1.9×10^{-5} mm/cycle). Crack propagation rates below this limit are 'near-threshold' that correspond to early stages of crack propagation where the threshold stress intensity factor range (ΔK_{TH}) is representative of the value below which the crack will not propagate [6]. However it should be noted that the lowest crack growth rates were higher for CMW1 than SmartSet GHV, because they largely describe crack growth in CMW1 specimens over the last few fatigue cycles before failure.

Fig. 8 shows the relationship between the crack growth rate and the stress intensity range for the two cements. The data obtained for the five data sets of each cement are plotted together with the regression line for each cement. The Paris' Law representative equations for these cements were

$\frac{da}{dN} = 2\times10^{7}\left(\Delta K\right)^{16.77}$ for CMW1 and $\frac{da}{dN} = 0.875\left(\Delta K\right)^{9.25}$ for SmartSet GHV. The lower number of data points for CMW1 in Fig. 8 reflects the effect of the fast crack growth reducing the number of data points for this cement due to the breakage of more than one gauge strand over a single fatigue cycle period, particularly during the later loading cycles.

Table 1 Comparison of fatigue crack lengths at the failure point for SmartSet GHV and CMW1 cements

	SmartSet GHV			CMW1		
Specimen No.	**Total cycles to failure (N_f)**	**No. of gauge strands broken at failure**	**Crack length at failure /mm**	**Total cycles to failure (N_f)**	**No. of gauge strands broken at failure**	**Crack length at failure /mm**
1	7,072	20*	~ 6.00	3,286	12	4.00
2	9,085	20*	~ 6.00	3,628	18	5.50
3	10,225	20	6.00	7,724	13	4.25
4	35,585	20	6.00	10,613	17	5.25
5	49,393	20*	~ 6.00	11,348	15	4.75

Failure of marked specimens (*) occurred at cycles to failure count just after that relevant to strand No. 20

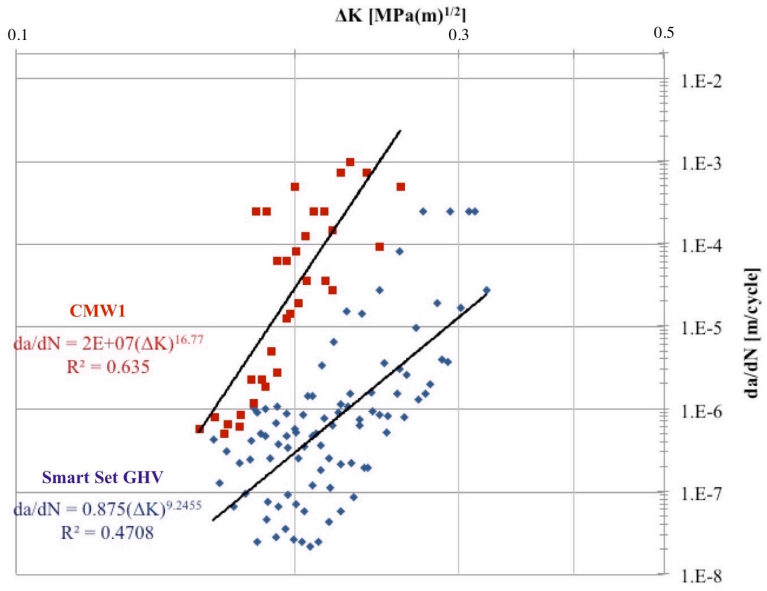

Figure 8 Summary of the da/dN versus ΔK_I results, with the best-fit to the Paris equation for SmartSet GHV (blue diamonds) and CMW1 (red squares).

4. Discussion

4.1 Absorbed energy as a fatigue damage indictor

Investigating the stress-strain curves of the specimen types for these two bone cements shows noticable differences between the fatigue crack damage progresses. At the higher stress levels the progressive change in the absorbed energy (shown by changes in the area of the stress-strain loops) indicated that crack growth behaviour is affected by specimen shape and production method. Furthermore, this effect of specimen type has been shown to be controlled simultaneously by the cement composition with greater differences between the SmartSet GHV and CMW1.

First of these factors is the interaction of specimen type and cement composition. In two of our previous [35,36] the differences in fatigue lives were attributed to variations in specimen production method and resultant surface morphology, leading to changes in the stress concentration factors and also considered the role of cement composition with limited discussion of crack propagation mechanisms. In our subsequent study [37], the specimen variables were examined further in a range of stress amplitudes, reporting a particular influence of the stress amplitude used in describing the fatigue longevity of different cements, without considering in depth the crack initiation and growth mechanisms. In the current study, the changes in absorbed energy per loading cycle are compared for different specimen types and the results have shown interesting findings regarding the effect of specimen type which are also controlled by cement composition. The results, according to the gradual increases in absorbed energy, indicate that SmartSet GHV cement is less resistant to fatigue damage with faster crack propagation, however the cracks initiated later. At high stress levels in particular, the machined specimens of this cement, especially the circular, were found to absorb more energy per load cycle starting in the earlier fatigue process compared to the moulded specimens; the trend becomes more obvious as the fatigue cycles progress, demonstrating that the machined specimens have low fatigue crack initiation and propagation resistance. In contrast, the absorbed energy of the all CMW1 cement specimen types remained constant throughout the early loading time and thus minimal crack initiation and propagation occurred. However, once the crack initiated the specimen showed almost immediate failure with no obvious resistance to crack propagation. Crack initiation also occurred earlier in the machined specimens compared to the moulded. This reflects the importance of cement composition and inclusions as being a leading factor in controlling the effect of specimen type on describing fatigue crack behaviour, but the similarity in crack growth trends, does not necessarily mean the fatigue lives are similar in vivo. The effect of machining the specimen surfaces which enhances the fatigue crack propagation in SmartSet GHV could be due to the molecular weight and bead size characteristics of this cement. Having different molecular weights and pre-polymerised polymer bead particle sizes, the speed of crack propagation in the two cements would differ, regardless of specimen type.

The effect of stress type and amplitude is also important. For the fully reversed tension-compression stress regimes, testing at a range of stress levels has shown significant variations in terms of the increase in absorbed energy rates. All CMW1 specimen types at all stress levels, revealed minimal increases in absorbed energy until a “close to failure” point. The results have also shown the change in stress amplitude within the examined range of stress levels leads to similar energy absorption behaviour for all specimen types, although variations occurred in the absorbed energy per fatigue cycle at different stress levels, leading to differences in the total fatigue lives. In contrast, SmartSet GHV results have shown clearly that there is a critical strain level that at or below which all specimen types can provide stable and low absorbed energy behaviour. However, exceeding this particular strain level can lead to clearer variations in terms of the increase in the absorbed energy amounts as the cyclic fatigue progresses. While this critical stress level has been shown to exist at somewhat lower levels for the machined specimens (apparently between ±15 and ±20 MPa), it appeared to be higher for the moulded specimens (between ±20 and ±30 MPa). The tension-tension testing at 2-20 MPa revealed a similar trend of difference in the absorbed energy and its changes for the two cements, it has also shown similar changes in all specimen types of the same cement. This finding might reflect the role that can stress type plays in crack initiation and propagation, based on the findings that tension-compression loading leads the specimen to absorb successively more energy than under tension-tension fatigue. This leads to the consideration of other possible factors that can exist when fatiguing specimens, such as sample temperature and creep.

One possible reason that might be involved in the dissimilar stress-strain behaviour of the two cement compositions at different stress types and amplitudes is the different impact that the stress level can have on the craze zones and their expected growth prior to crack propagation. It has been stated for polymers that “the craze crack growth increases with stress” [42]. This, however, does not necessarily mean subsequent gradual crack growth since, as it has been demonstrated by Kambour [15] for the stress-strain behaviour of the craze in glassy polymers, the craze can be “much softer than the parent polymer, but capable of sustaining larger stresses and strains up to the point of failure” whereas, in this case, “craze failure is much more dependent on polymer molecular weight than craze formation”. These suppositions seem to apply to the stress-stain behaviour in the current study, for both stress types tested and is more apparent at high stress levels, such that CMW1 can sustain stresses without gradual crack growth whereas, in contrast, crazes in SmartSet GHV progress steadily, but start earlier, well before failure.

In addition to the consideration of specimen specifications and stress parameters, the thermal properties of test specimens may also play a role. The general concept is that in polymers higher fatigue stress levels lead to an increase in the hysteresis generated heat [25]. The extent of thermal heating is controlled by the size of the stressed component, the heat loss from the surface area of the specimen and the flow rate of any fluid, such that the lower the surface area to volume ratio the greater the accumulated heating. For specimens used in the current study, the surface area to volume ratios are 0.8 and 0.9 for the circular and the rectangular specimens respectively, thus reasonably close. The temperature was controlled by flowing saline at 37˚C over the samples and although the flow rate was not measured there was significant fluid flow which should have reduced sample heating. Considering the cement composition, the difference in opacifier filler is less likely to show dissimilar thermal stability since both fillers (ZrO_2 and $BaSO_4$) are ceramics and have similar thermal properties. Considering added antibiotics, while it has been reported by Webb and Spencer [44] that a number of antibiotics such as flucloxacillin, penicillin, chloramphenicol and tetracycline are heat labile, Gogia et al. [9] also reported that one of the basic considerations for antibiotics to be used in bone cement is to be heat stable. Gentamicin sulphate, in particular, is said to have "good thermostability"[18], thus unlikely to influence the thermal stability of SmartSet GHV either during polymerisation or fatigue loading. Thus any differences in thermal stability, would therefore be due to other variables including the difference between the basic polymer structures of the cements. The powder in CMW1 is poly(methyl methacrylate) while SmartSet GHV is a copolymer of poly(methyl methacrylate with methacrylate), although the relative amounts of each are not stated. The glass transition temperatures for poly(methyl methacrylate) (PMMA) and poly(methyl acrylate) (PMA) are 105˚C and 6˚C, respectively [7]. Changes in the specific heat capacity at these temperatures were reported, in the same study, as 33.5 and 42.3 J mol^{-1} K^{-1}, respectively. According to the stress-strain behaviours of both cements, the variations in thermodynamic properties would be stress amplitude dependant, and would be more obvious in SmartSet GHV specimens.

The contribution of creep in controlling fatigue crack growth has also been considered. Examining tensile fatigue damage in the cement-bone interface, Kim et al [16] reported that fatigue creep dominates the stiffness changes. In the current study, the tension-tension stress-strain responses for all specimen types indicated that the creep properties seem to be governed by cement composition. The hysteresis loop movement along the strain axis of the stress-strain plots was previously reported in Sheafi and Tanner [36], the SmartSet GHV specimens, tend to undergo approximately 3 times more creep than the CMW1 specimens (Fig. 5), which can also be related to the development of fatigue damage. The circular machined specimens of this cement failed earlier, but the creep trend was similar to the early stages of the other specimen types. Considering the test environment, Liu et al. [26] found that SmartSet GHV undergoes about four times as much creep at body temperature than at room temperature, whereas Simplex P the difference was a factor of less than two. For CMW1 specimens, the creep behaviour is similar in all specimens, with substantially lower creep rates than SmartSet GHV. While the creep appeared to be greater in SmartSet GHV, this indicates that creep might have contributed to increasing the fatigue life, but was not necessarily the dominant factor. The possibility of creep affecting fatigue longevity in tension cannot be relied on for making final conclusions since only a single tension-tension stress level has been tested. It has been reported in other studies that the correlation between fatigue life and creep of bone cement is stress level dependent. Verdonschot and Huiskes [41], for instance, testing in compression concluded that higher fatigue stress levels lead to higher creep rates. While Waanders et al. [43] suggested that, for the cement-bone interface damage mechanics, "at higher external stresses, creep is not capable of relieving peak cement stresses to such an extent that fatigue crack formation is attenuated", they referred to the increased contribution of creep in fatigue crack formation at lower stress levels. If this was the case, the more stable crack propagation found for the lower stress levels of the tension-compression regimes (mainly for SmartSet GHV) would be attributed, at least in part, to creep. Overall, however, while the effect of creep on fatigue crack propagation cannot be totally neglected further investigations are still required to compare the effect of applying tension-tension at different stress levels and noting that tensile hoop stresses are generated around an implant stem.

4.2 Fatigue crack growth in CT specimens

Race and Mann [32] proposed that two-power law fits are required to represent fatigue crack propagation rates in PMMA bone cement. Examining their findings along with those of Monlino and Topoleski [28] and Nguyen et al. [29], they believed that the existence of "discontinuities in the log-log plot of da/dN versus ΔK" is unavoidable and the data cannot be reduced to a single power law. It should be noted though, of these three studies, only Monlino and Topoleski [28] examined Simplex P along with radiolucent Simplex P and Plexiglas® while the other two studies examined the crack growth in Simplex P only. This is important since, as described by Bialoblocka-Juszczyk et al. [4], the fracture properties of bone cement can be influenced by its chemical composition and the testing procedures. Bialoblocka-Juszczyk et al. [4] measured the fatigue crack propagation in Cemex® RX considering it to be "representative of a standard PMMA based bone cement". They used the data of five specimens to generate a single regression line described by Paris' law, obtaining a general coefficient of regression of 0.96. Two different PMMAs, rather than PMMA based bone cement, were tested by Hao et al. [11] using both compact tension (CT) and middle tension (MT) fracture toughness samples. Using CT samples they found that there was minimal differences between the two cements, but using the MT there was an obvious difference in the gradients of the da/dN versus ΔK graphs, thus indicating difference in the Paris Law equations.

One consideration in the current study was that a precise and correct identification of the "area of interest" during which the crack propagation would be driven by the stress intensity factor (macrocrack growth) and neglecting data points close to the crack tip of the CT specimen which perhaps can lead to both reporting more representative results and providing a greater chance to obtain a single linear fit of data points on a log-log graph. The coefficient of regression (R^2) obtained from the da/dN versus ΔK plot for each specimen individually (not shown) was high (up to 0.98) for the data sets of many specimens and although a few sets showed low coefficients (down to 0.35). The individual plots which provided high regression coefficients might indicate that the Paris' law is followed over the area examined. The combination of the cement data sets (Fig. 8) to give a single trend line as suggested by Bucci [6]. Ginebra et al. [8] and Bialoblocka-Juszczyk et al. [4] indicates that these two cements have distinct fracture behaviours. The combined data of CMW1 has also indicated that the change in stress intensity range occurs at a higher crack length compared to SmartSet GHV, with a higher gradient for CMW1 (i.e. lower crack growth resistance). This dissimilarity in behaviour was perhaps because, as discussed earlier, CMW1 has an increased ability to resist crack initiation and growth, indicating delayed threshold stress intensity factor range (ΔK_{TH}), followed by sudden and rapid crack propagation. Overall, the use of Paris' power law to examine fatigue crack growth in bone cement depends on the cement composition such that it can be adequate and applicable for specific cements, suggests that the testing protocol is appropriate.

The molecular characteristics, including molecular weight and molecular weight distribution, are important in influencing the advancement of fatigue crack through the craze zone where higher molecular weight leads to increased craze strength [31]. For bone cement, the formation of the craze zones is influenced by the molecular weight such that increasing the molecular weight increases the fracture resistance [33]. Liu et al [27] reported that SmartSet GHV and CMW1 have similar narrow bead size distributions and that the mean diameters were 69 ± 2.1 and 44 ± 1.9 μm for SmartSet GHV and CMW1, respectively. SmartSet GHV powder has substantially greater molecular weight compared to CMW1 powder ($\sim 1\times10^6$ and 2×10^5 g/mol, respectively), however, the reverse is true for the molecular weights of the cements matrices ($\sim 5.5\times10^5$ and 9×10^5 g/mol, respectively). Variations in the molecular weights of both the matrices and the powder will have an important effect on the fatigue crack growth and through which phases of the material the crack will travel. Kim et al. [17] observed for polymethylmethacrylate in particular, increasing the molecular weight from 1×10^5 to 4.8×10^6 g/mol led to a decrease in fatigue fracture growth rates by two orders of magnitude. It has been reported that while the reduction in molecular weight lowers fracture toughness, this does not necessarily lead to shorter fatigue life, but a decline in fatigue lives may occur if the molecular weight is greatly reduced [10]. Therefore, on the one hand, the higher molecular weight for CMW1 matrix (approximately 1.6 times greater than SmartSet GHV) can be considered a possible reason for these variations in the fatigue crack growth behaviour between the two cements, particularly in terms of controlling the time to start crack

propagation, while, on the other hand, the total fatigue life results, as reported in our previous studies [35,36], does not reflect this clear difference in crack propagation behaviour between the two cements.

Liu et al. [26] also considered the mechanical characteristics of SmartSet GHV and stated "it is evident that most of the micro-cracks propagate around large PMMA beads, indicating a weak bonding between the large beads and the matrix". This finding matches our observations of the fracture surfaces of SmartSet GHV. Debonding of the PMMA beads from the matrix in the SmartSet GHV fracture surfaces was much more obvious (Fig. 6a) as the opacifier particles accumulate around the larger beads (Fig. 6b). In comparison CMW1 which showed no obvious beads or disconnections at comparable magnification levels and the crack has propagated through the original PMMA beads (Fig. 6c and 6d, respectively), leading to the rougher fracture surfaces for the SmartSet GHV. Theoretically, this is possible since the lower fraction and the smaller size of CMW1 PMMA beads would be expected to exhibit greater matrix-bead bonding, resulting in superior resistance to crack growth. The effect of the antibiotic is difficult to define due to the other differences between these two cements. Rimnac et al. [34] compared the fracture properties of different commercial bone cements each with and without antibiotic and attributed the variations in fracture toughness and fatigue crack propagation to the difference in molecular weights with no significant effect from the presence of antibiotics.

In brief, the differences in both molecular weight and PMMA beads characteristics can be considered among the main factors that govern fatigue fracture. Compared to CMW1, the lower molecular weight of SmartSet GHV matrix and the greater size of the PMMA beads within its structure seem to play a key role in producing slow fatigue crack propagation starting from earlier fatigue loading cycles. This means the crack would preferably grow within the weaker matrix extending through the bead-matrix interface as being the second weakest route. The occasional presence of accumulated opacifier, particularly adjacent to the beads, may have a contributing effect on crack behaviour. Contrary to SmartSet GHV, the higher matrix molecular weight and the greater bonding between the PMMA beads and matrix in CMW1 can delay the crack progress within the bulk structure. However, once the crack has started to progress in this cement the bonding between the pre-polymerised beads and the matrix will no longer resist the crack propagation where a rapid increase in crack growth rate occurs over few cycles, leading to fast failure.

Conclusions

1. For all testing regimes used in this study, the increase in absorbed energy per loading cycle is much greater for SmartSet GHV than CMW1, thus reflecting the earlier initiation but more gradual crack propagation in SmartSet GHV leading to slow failure.
2. For the examined fully reversed tension-compression stress levels, the increase in stress upon SmartSet GHV specimens above a certain level can lead to extremely rapid increase in the absorbed energy (i.e. more immediate fatigue damage). This changeover stress level, however, can be comparatively influenced by the specimen type, with the machined specimens being the most affected. In contrast, all CMW1 specimens, at every stress level, tend to absorb a similar amount of energy throughout the fatigue loading period until close to failure.
3. The direct measurements of the crack growth rates in SmartSet GHV and CMW1, using the ASTM E647-13 compact tension standard technique, have validated the equivalent stress-strain (energy absorption) findings in terms of the difference in crack propagation behaviour of both cements. Again, the cracks tend to progress gradually in SmartSet GHV from well before failure while showing no clear propagation in CMW1 and then sudden failure.
4. These different cements show different compliance to Paris' power law. The application can be much more suitable for particular cements (such as SmartSet GHV) than others (as CMW1). Whether or not the cement was following Paris' law, the application would still be of help in, at least, identifying if the crack propagation would at some stage be in agreement with this law.
5. Overall, while the cement composition and stress parameters are essential in identifying the fatigue crack propagation behaviour, there is still some uncertainty about what underlying factors are dominant in governing the propagation process. Although thermal properties and creep can possibly affect the crack propagation behaviour, it is suggested that the differences in molecular weight of the matrix and PMMA particle characteristics of the cements are likely to have the key role in controlling the crack growth progress.

Acknowledgements

The authors thank DePuy CMW for providing the bone cement materials and mixing devices. The Libyan Government is acknowledged for funding the research (PhD studentship ref 6978).

References

1. ASTM E647-13 2013. Standard Test Method for Measurement of Fatigue Crack Growth Rates. ASTM International, West Conshohocken, PA, USA
2. ASTM F2118 - 03 2003. Test Method for Constant Amplitude of Force Controlled Fatigue Testing of Acrylic Bone Cement Materials. ASTM International, West Conshohocken, PA, USA
3. ASTM F2118 - 14 2014. Standard Test Method for Constant Amplitude of Force Controlled Fatigue Testing of Acrylic Bone Cement Materials. ASTM International, West Conshohocken, PA, USA
4. Bialoblocka-Juszczyk, E., Baleani, M., Cristofolini, L. & Viceconti, M. 2008. Fracture properties of an acrylic bone cement. *Acta of Bioengineering and Biomechanics,* 10, 21-26.
5. Britton, J. R., Walsh, L. A. & Prendergast, P. J. 2003. Mechanical simulation of muscle loading on the proximal femur: analysis of cemented femoral components migration with and without muscle loading. *Clinical Biomechanics (Bristol; Avon),* 18, 637-646. DOI: 10.1016/S0268-0033(03)00113-X
6. Bucci, R. J. 1981. Development of a Proposed ASTM Standard Test Methods for Near-Threshold Fatigue Crack Growth Rate Measurment *In:* Hudak, S. J. & Bucci, R. J. (eds.) *Fatigue Crack Growth Measurment and Data Analysis.* Philadelphia, US: American Society for Testing and Materials
7. Gaur, U., Lau, S., Wunderlich, B. B. & Wunderlich, B. 1982. Heat capacity and other thermodynamic properties of linear macromolecules: 6. Acrylic polymers. *Journal of Physical and Chemical Reference Data* 11, 1065-1089. DOI: 10.1063/1.555671
8. Ginebra, M. P., Albuixech, L., Fernandez-Barragan, E., Aparicio, C., Gil, F. J., San Roman, J., Vazquez, B. & Planell, J. A. 2002. Mechanical performance of acrylic bone cements containing different radiopacifying agents. *Biomaterials,* 23, 1873-1882. DOI: 10.1016/S0142-9612(01)00314-3
9. Gogia, J. S., Meehan, J. P., Di Cesare, P. E. & Jamali, A. A. 2009. Local antibiotic therapy in osteomyelitis. *Seminars in Pastic Sugery,* 23, 100-107. DOI: 10.1055/s-0029-1214162
10. Graham, J., Pruitt, L., Ries, M. & Gundiah, N. 2000. Fracture and fatigue properties of acrylic bone cement - The effects of mixing method, sterilization treatment, and molecular weight. *Journal of Arthroplasty,* 15, 1028-1035. DOI: 10.1054/arth.2000.8188
11. Hao, W., Ma, L.T., Chen, X.W., Yuan, Y.N., Ma, Y.J. 2016. Comparison of the Fatigue Crack Propagation Behavior of Two Different Forms of PMMA Using Two-Stage Zone Model. *Journal of Materials Engineering and Performance* 25(1), 493-501 DOI: 10.1007/s11665-015-1852-z
12. Harper, E. J. & Bonfield, W. 2000. Tensile characteristics of ten commercial acrylic bone cements. *Journal of Biomedical Materials Research* 53(15), 605-616. DOI: 10.1002/1097-4636(200009)53:5<605::AID-JBM22>3.0.CO;2-5
13. Jasty, M., Maloney, W.J., Bragdon, C.R., O'Connor, D.O., Haire, T. & Harris, W.H. 1991. The initiation of failure in cemented femoral components of hip arthroplasties. *Journal of Bone and Joint Surgery [Br]*, 73-B, 551-558.
14. Jeffers, J.R.T., Browne, M., Taylor, M. 2005. Damage accumulation, fatigue and creep behaviour of vacuum mixed bone cement. *Biomaterials*, 26, 5532-5541. DOI: 10.1016/j.biomaterials.2005.02.009

15. Kambour, R. P. 1968. Stress-strain behaviour of the craze. *Polymer Engineering and Science,* 8, 281-289. DOI: 10.1002/pen.760080408
16. Kim, D. G., Miller, M. A. & Mann, K. A. 2004. Creep dominates tensile fatigue damage of the cement-bone interface. *Journal of Orthopaedic Research,* 22, 633-40. DOI: 10.1016/j.orthres.2003.09.007
17. Kim, S. L., Skibo, M., Manson, J. A. & Hertzberg, R. W. 1977. Fatigue crack propagation in poly(methyl methacrylate): Effects of molecular weight and internal plasticization. *Polymer Engineering & Science*, 17, 194-203.
18. Klemm, K. 2001. The use of antibiotic-containing bead chains in the treatment of chronic bone infections. *Clinical Microbiology and Infection,* 7, 28-31. DOI: 10.1046/j.1469-0691.2001.00186.x
19. Kühn, K.-D., Bone Cements, 2nd Edition, Published by Springer-Verlag, Berlin, Germany, 2014.
20. Lennon, A. B. & Prendergast, P. J. 2005. Evaluation of cement stresses in finite element analysis of cemented orthopaedic implants. *Journal of Biomedical Engineering,* 123, 623-628. DOI:10.1115/1.1412452
21. Lewis, G. 2003. Fatigue testing and performance of acrylic bone-cement materials: state-of-the-art review. *Journal of Biomedical Materials Research Part B: Applied Biomaterials* 66B, 457-486. DOI: 10.1002/jbm.b.10018
22. Lewis, G. & Nyman, J.S. 2000. Toward standardization of methods of determination of fracture properties of acrylic bone cementand statistical analysis of test results. *Journal of Biomedical Materials Research* 53**,** 748-768 DOI: 10.1002/1097-4636(2000)53:6<748::AID-JBM18>3.0.CO;2-Z
23. Lewis, G., van Hooy-Corstjens, C. S., Bhattaram, A. & Koole, L. H. 2005. Influence of the radiopacifier in an acrylic bone cement on its mechanical, thermal, and physical properties: barium sulfate-containing cement versus iodine-containing cement. *Journal of Biomedical Materials Research Part B: Applied Biomaterials,* 73, 77-87. DOI: 10.1002/jbm.b.30176
24. Lewis, G., Wellborn, B., Jones, L., Biggs, P. 2009. A room-temperature autonomically-healing PMMA bone cement: influence of composition on fatigue crack propagation rate. *Journal of Applied Biomaterials & Biomechanics*. 7, 90-96.
25. Liu, A. F. 2005. *Mechanics and Mechanisms of Fracture: An Introduction* USA, ASM International
26. Liu, C. Z., Green, S. M., Watkins, N. D., Baker, D. & McCaskie, A. W. 2005. Dynamic creep and mechanical characteristics of SmartSet GHV bone cement. *Journal of Materials Science: Materials in Medicine,* 16, 153-160. DOI: 10.1007/s10856-005-5893-y
27. Liu, C. Z., Green, S. M., Watkins, N. D., Gregg, P. J. & McCaskie, A. W. 2002. Creep behaviour of CMW1 and Palacos R-40 clinical bone cements. *Journal of Materials Science: Materials in Medicine*, 13, 1021-1028. DOI: 10.1023/A:1020328218520
28. Molino, L. N. & Topoleski, L. D. 1996. Effect of $BaSO_4$ on the fatigue crack propagation rate of PMMA bone cement. *Journal of Biomedical Materials Research,* 31, 131-137. DOI: 10.1002/(SICI)1097-4636(199605)31:1<131::AID-JBM14>3.0.CO;2-Q
29. Nguyen, N. C., Maloney, W. J. & Dauskardt, R. H. 1997. Reliability of PMMA bone cement fixation: fracture and fatigue crack-growth behaviour. *Journal of Materials Science: Materials in Medicine,* 8, 473-483. DOI: 10.1023/A:1018574109544
30. Paz, E., Forriol, F., del Real, J. C., Dunne, N. 2017 Graphene oxide versus graphene for optimisation of PMMA bone cement for orthopaedic applications. *Materials Science and Engineering C - Materials for Biological Applications*, 77, 1003-1011. DOI: 10.1016/j.msec.2017.03.269.
31. Pruitt, L. A. 2003. Fatigue testing and behaviour. *In:* Lampman, S. (ed.) *Characterization and Failure Analysis of plastics.* USA: ASM International.
32. Race, A. & Mann, K. A. 2008. Fatigue crack propagation rates in PMMA bone cement cannot be reduced to a single power law. *Journal of Biomedical Materials Research Part B: Applied Biomaterials,* 86, 278-282. DOI: 10.1002/jbm.b.31016
33. Ries, M. D., Young, E., Al-Marashi, L., Goldstein, P., Hetherington, A., Petrie, T. & Pruitt, L. 2006. In vivo behaviour of acrylic bone cement in total hip arthroplasty. *Biomaterials,* 27, 256-261. DOI: 10.1016/j.biomaterials.2005.05.103
34. Rimnac, C.M., Wright, T. M.., McGill, D.L. 1986. The effect of centrifugation on the fracture properties of acrylic bone cements. *Journal of Bone and Joint Surgery [Am]*, 68A, 281-287. DOI: 10.2106/00004623-198668020-00014
35. Sheafi, E. M. & Tanner, K. E. 2014. Effects of test sample shape and surface production method on the fatigue behaviour of bone cement. *Journal of the Mechanical Behavior of Biomedical Materials,* 29, 91-102. DOI: 10.1016/j.jmbbm.2013.08.023
36. Sheafi, E. M. & Tanner, K. E. 2015. Influence of test specimen fabrication method and cross-section configuration on tension–tension fatigue life of PMMA bone cement. *Journal of the Mechanical Behavior of Biomedical Materials*, 51, 380-387. DOI: 10.1016/j.jmbbm.2015.07.024
37. Sheafi, E. M. & Tanner, K. E. 2017. Effects of specimen variables and stress amplitude on the S-N analysis of two PMMA based bone cements. *International Journal of Fatigue*, 105, 119-127. DOI: 10.1016/j.ijfatigue.2017.08.019
38. Tanner, K. E., Wang, J.-S., Kjellson, F. & Lidgren, L. 2010 Comparison of two methods of fatigue testing of bone cement. *Acta Biomaterialia*, 6, 943-952. DOI: 10.1016/j.actbio.2009.09.009
39. Topoleski, L. D. T., Ducheyne, P., Cuckler, J. M. 1990. A fractographic analysis of in vivo poly(methyl methacrylate) bone-cement failure mechanisms. *Journal of Biomedical Materials Research*, 24, 135-154. DOI: 10.1002/jbm.820240202
40. van Hooy-Corstjens, C. S. J., Govaert, L. E., Spoelstra, A. B., Bulstra, G. M. R., Wetzels, G. M. R., Koole, L. H. 2004. Mechanical behaviour of a new acrylic radiopaque iodine-containing bone cement. *Biomaterials*, 25, 2657-2667. DOI: 10.1016/j.biomaterials.2003.09.038
41. Verdonschot, N. & Huiskes, R. 1995. Dynamic creep behaviour of acrylic bone cement. *Journal of Biomedical Materials Research,* 29, 575-581. DOI: 10.1002/jbm.820290504
42. Volynskii, A. L. & Bakeev, N. F. 1995. *Solvent Crazing of polymers,* **Pub** Elsevier science B. V., Amsterdam, The Netherlands,
43. Waanders, D., Janssen, D., Mann, K. A. & Verdonschot, N. 2010. The effect of cement creep and cement fatigue damage on the micromechanics of the cement-bone interface. *Journal of Biomechanics,* 43, 3028-3034. DOI: 10.1016/j.jbiomech.2010.06.031
44. Webb, J. C. J. & Spencer, R. F. 2007. The role of polymethylmethacrylate bone cement in modern orthopaedic surgery. *Journal of Bone and Joint Surgery [Br],* 89-B, 851-857. DOI: 10.1302/0301-620X.89B7.19148
45. Wheeler, J.P.G, Miles, A.W. & Clift, S.E. 1999. The influence of the time-dependent properties of bone cement on stress in the femoral cement mantle of total hip arthroplasty. *Journal of Materials Science: Materials in Medicine,* 10, 497-501. DOI: 10.1023/A:1008957227452